International Journal of Disaster Risk Science
https://doi.org/10.1007/s13753-026-00696-z

www.ijdrs.com
www.springer.com/13753

ARTICLE

Optimal Seismic Intensity Measures for Slopes at Various Heights Under Vertical and Horizontal Ground Motions

Dung Thi Phuong Tran[1,2] · Hoang D. Nguyen[3] · Jianbo Fei[1,2] · Muhammad Irslan Khalid[1,2] · Xiangsheng Chen[1,2]

Accepted: 6 December 2025

Abstract

Identifying the optimal intensity measures (IMs) of ground motion is a critical step in the seismic fragility analysis of slopes using probabilistic seismic demand models. In this study, we investigated various IMs of earthquake ground motions, considering both vertical and horizontal components that can trigger landslides, through numerical simulations. A set of 19 IMs was examined for three heights of slopes. The optimal IMs were assessed using the maximum permanent displacement as an engineering demand parameter. The findings reveal that acceleration-related parameters specifically sustained maximum acceleration (SMA) and root-mean-square of acceleration, and velocity-related parameters namely sustained maximum velocity (SMV) and peak ground velocity, are the most effective IMs for slopes subjected to both vertical and horizontal ground motions. For slopes subjected exclusively to horizontal ground motion, SMA is recommended as the optimal IM for lower-height slopes, while SMV is more suitable for the taller slope. In contrast, for models subjected to combined horizontal and vertical ground motions, SMA is consistently identified as the optimal IM for slope across all heights. Notably, the study concludes that peak ground acceleration, a commonly used parameter in seismic analysis, is unsuitable for the considered slopes.

Keywords Ground motion components · Intensity measures · PSDMs · Seismic fragility · Slopes

1 Introduction

Seismic fragility analysis is critical for analyzing slope failure susceptibility in geotechnical structures like roadway embankments, dams, bridge abutments, and lifeline infrastructure in mountainous regions (Crowley et al. 2004; Saygili and Rathje 2009; Tsompanakis et al. 2010; Kim and Sitar 2013; Nguyen et al. 2020; Nguyen et al. 2024). It uses earthquake hazard data to analyze slope stability and estimate damage, aiding managers to reduce seismic risks. Fragility analysis estimates structure damage based on capacity limit and intensity measure (IM) of ground motion (Maruyama et al. 2010; Wu 2014; Hu et al. 2019; Tran et al. 2023; Khalid et al. 2024; Kim et al. 2025). Developing a fragility curve for geotechnical structures subjected to earthquake requires a relationship between structural seismic demand (SSD) and given IM. Nonlinear time-history analysis is usually used to construct a probabilistic seismic demand model (PSDM) for this empirical relationship.

Employing PSDM to develop a fragility curve is necessary to select both the SSD and an appropriate IM. Performance of a seismic slope is typically evaluated in terms of seismically induced maximum permanent displacement (D_{max}), as seismic slope stability. Several studies have computed D_{max} for slopes and correlated it with parameters characterizing the IM at the site of interest. For instance, Fotopoulou and Pitilakis (2015) conducted numerical parametric analyses using FLAC-2D to evaluate D_{max} against IMs of peak ground acceleration (PGA), peak ground velocity (PGV), and Arias intensity (I_A). Saygili and Rathje (2008) presented a scalar model to predict sliding displacement against PGA and the yield coefficient k_y. However, it is unclear whether these parameters are the best among the

✉ Jianbo Fei
feijianbo@szu.edu.cn

1 State Key Laboratory of Intelligent Geotechnics and Tunnelling, Shenzhen University, Shenzhen 518060, China

2 Key Laboratory for Resilient Infrastructures of Coastal Cities (MOE), Shenzhen University, Shenzhen 518060, China

3 Department of Civil and Environmental Engineering, Faculty of Engineering, University of Alberta, Edmonton, AB T6G 1H9, Canada

Published online: 23 January 2026

many feasible alternatives (Alielahi and Moghadam 2016; Hariri-Ardebili and Saouma 2016).

The most common IMs, like PGA, PGV, and peak ground displacement (PGD), determine the maximum absolute values from acceleration, velocity, and displacement time histories (Trifunac and Brady 1975). Additionally, there are less frequently used acceleration-related IMs, including I_A (Arias 1970), characteristic intensity (I_C) (Park et al. 1985), root-mean-square acceleration (a_{RMS}) (Kramer 1996), and sustained maximum acceleration (SMA) (Nuttli 1979). Velocity- and displacement-related IMs have been defined, including root-mean-square velocity (v_{RMS}) (Housner 1975), sustained maximum velocity (SMV) (Nuttli 1979), cumulative absolute velocity (CAV) (Reed and Kassawara 1990), cumulative absolute displacement (CAD) (Mackie and Stojadinović 2001), and root-mean-square displacement (d_{RMS}) (Riddell and Garcia 2001). Furthermore, IMs derived from response spectra were proposed, consisting acceleration spectrum intensity (ASI) (Thun et al. 1988), velocity spectrum intensity (VSI) (Thun et al. 1988), Housner intensity (HI) (Housner 1975), effective peak acceleration (EPA) (Kurama and Farrow 2003), and spectral acceleration, velocity, and displacement at the first natural period (Shome et al. 1998). More information and methodologies for determining IMs can be found in studies such as Hariri-Ardebili and Saouma (2016) and Kramer (1996).

Several studies have analyzed various IMs and selected optimal IMs for different structures. Hariri-Ardebili and Saouma (2016) investigated 70 IMs across seven categories in PSDM of a concrete dam, utilizing four criteria—efficiency, practicality, proficiency, and sufficiency—to compute the optimal IM for 100 analyzed ground motions. Considering the crest displacement as the SSD, they proposed optimal IMs for each category: PGV was identified as the optimal IM for ground motion-dependent scalar IMs; Fajfar intensity (IF), which is a compound IM that acknowledges the damage capacity of medium-period structures, was optimal for ground motion-dependent compound. Zhang et al. (2022) conducted a study to determine optimal IMs in PSDM for various burial depths of a subway station. They simulated a three-story, three-span subway station subjected to 100 horizontal ground motions, computing the maximum inter-story drift ratio (MIDR). They selected 21 IMs divided into two groups: non-structure-specific IMs (sub-groups of acceleration-, velocity-, and displacement-related) and structure-specific IMs. The results suggested that for a subway station embedded in site class 2 (SC2 includes density $\rho = 1950$ kg/m^3, initial shear modulus $G = 2.8\times10^8$ Pa, shear velocity $V_{s30} = 377$ m/s, Poisson's ratio $\mu = 0.38$, cohesion $c = 3.5\times10^4$ Pa, and frictional angle $\varphi = 13°$), VSI was optimal at every burial depth, while for a station embedded in SC3 (the site class with $\rho = 1950$ kg/m^3, $G = 8.8\times10^8$ Pa, $V_{s30} = 212$ m/s, $\mu = 0.33$, $c = 1.4\times10^4$ Pa, and $\varphi = 23°$), PGV and VSI were optimal at a burial depth of 4 m, while VSI and IF were optimal at depths of 8 m and 20 m, respectively. Travasarou and Bray (2003) correlated D_{max} with 12 IMs obtained from 1447 horizontal ground motions to define optimal IMs for stiff slopes by linear and nonlinear regression analyses. They considered the criteria of efficiency and sufficiency in IM analysis. The results showed that I_A was a good IM for stiff slopes in the equivalent-linear model, whereas spectral acceleration at the slope's elastic fundamental period (SA) was the best IM for the linear model. More studies were found in the determination of ground motion IMs for various geotechnical structures (Che et al. 2023; Irslan Khalid et al. 2023; Nguyen, Shin, et al. 2023).

Few studies have addressed the selection of appropriate IMs for slopes, especially with vertical ground motions considering PSDM. Numerous seismic fragility studies used PGA as an IM; however, some research suggests that it may not be suitable (Travasarou and Bray 2003; Nguyen et al. 2021; Hu and Bao 2024). Furthermore, optimal IMs may vary with some conditions including slope geometry (for example, slope height and inclination) (Che et al. 2023), the ground motion (Padgett et al. 2007), and site conditions (Zhang et al. 2022). This study addressed these research gaps by adopting a unique approach to selecting the best IM for evaluating slope D_{max} under various seismic situations to improve seismic risk assessments. The study evaluated slopes of 10, 20, and 30 m high to reveal how seismic responses vary with slope geometry, a topic rarely studied. The study also incorporated vertical and horizontal ground motions, providing a more complete knowledge of seismic influences on slopes than horizontal-only analyses. Advanced analytical and numerical modeling techniques of finite element methods in PLAXIS-2D accurately simulate slope behavior for seismic inputs, advancing seismic slope stability analysis. Finally, the article presents the best IM for slope stability assessments based on the engineering demand parameter (EDP) of D_{max}. These findings provide useful guidance for engineers in seismic slope design and risk assessment.

2 Methodology

This section describes PSDMs that establish statistical relationships between an IM and structural responses (for example, D_{max} of slopes) to provide a comprehensive understanding of seismic vulnerability levels. It also lists four criteria for choosing the best IM: efficiency, practicality, proficiency, and sufficiency. The chosen IM is accurate and dependable for seismic slope failure evaluations.

2.1 Probabilistic Seismic Demand Models (PSDMs)

Probabilistic seismic demand models are significant in the study of seismic fragility of slopes because they establish a relationship between D_{max} and IMs such as PGA during the first natural period. They are conditional probability functions (P[D>C|IM]) expressing the likelihood that a slope will have a certain demand (D) given an IM (Tran et al. 2023). Previous studies (Cornell et al. 2002; Padgett and DesRoches 2008; Hariri-Ardebili and Saouma 2016; Nguyen, Lee, et al. 2023) assumed that this conditional probability function follows a lognormal distribution, as Eq. 1:

$$P[D \geq C|\mathrm{IM}] = \Phi\left[\frac{\ln\left(S_{D|\mathrm{IM}}/S_{\mathrm{C}}\right)}{\beta_{\mathrm{total}}}\right] \tag{1}$$

$$\beta_{\mathrm{total}} = \sqrt{\beta_{D|\mathrm{IM}}^2 + \beta_C^2 + \beta_{\mathrm{M}}^2} \tag{2}$$

where $P[\cdot]$ is the probability of exceeding the limit state of the seismic demand D (the D_{max} computed from the nonlinear time history analyses), and C is the capacity of the slope. $S_{\mathrm{D|IM}}$ is the median infrastructural demand associated with IM. S_{C} is the threshold value of the limit state, $\beta_{\mathrm{D|IM}}$ is the logarithmic standard deviation of the seismic demand, β_{C} is the logarithmic standard deviation accounting for the uncertainty in the limit state, and β_{M} is the logarithmic standard deviation describing the uncertainty modeling. In this study, the D_{max} of the slope was considered as the seismic demand (also known as the EDP) in PSDM. The relationship between D_{max} and IM can be expressed as follows:

$$\ln(D_{max}) = \ln(a) + b \times \ln(\mathrm{IM}) \tag{3}$$

where a and b are the coefficients derived from the regression analysis. We considered β_{C} and β_{M} to be 0.3 and 0.4, respectively, as suggested by Wen et al. (2004) and HAZUS-MH (NIBS and FEMA 2003). $\beta_{D|IM}$ is calculated using the regression analysis and seismic demand of the slope following Eq. 4:

$$\beta_{D|\mathrm{IM}} \cong \sqrt{\frac{\sum\left(\ln\left(d_i\right) - \ln\left(a \times \mathrm{IM}^b\right)\right)^2}{N-2}} \tag{4}$$

where d_i is the D_{max} of the slope subjected to ground motion number i ($i = 1, \ldots, N$). N is the total number of ground motions.

Using the D_{max}, this study analyzed 19 ground motion IMs to find the best one for slope seismic fragility analysis. The following steps should be taken to create a PSDM: First, the number of N ground motions and their IMs are chosen. Second, a numerical model of the slope is built, and nonlinear history analyses are performed on this model exposed to N ground motions to determine D_{max}. After that, we conducted a linear regression analysis between D_{max} and the IMs to obtain the coefficients as shown in Eq. 3. Finally, Eq. 1 is used to develop the fragility curve of the slope, considering the capacity limit state of S_{C}. Two major benefits result from correlating seismically produced D_{max} with an IM indicating strong ground motion intensity. First, optimal IM improves displacement prediction, lowering ground motion for dynamic response analysis. Correlating IM and displacement in a simplified manner improves displacement prediction. Second, the dynamic response assessment can be isolated from seismic hazard computation, allowing probabilistic seismic evaluations to use widely available seismic hazard maps.

2.2 Criteria for the Selection of Optimal Intensity Measures

This study considered four criteria to determine the optimal IM including efficiency, practicality, proficiency, and sufficiency (Hariri-Ardebili and Saouma 2016; Tidke and Adhikary 2022; Nguyen, Shin, et al. 2023). Each criterion is briefly defined as follows.

2.2.1 Efficiency

An efficient IM is characterized by reduced dispersion of D_{max} for a given IM. This efficiency can be quantified using $\beta_{\mathrm{D|IM}}$ from Eq. 4, which represents the standard deviation of the structural demand for a specified IM. Consequently, a lower $\beta_{\mathrm{D|IM}}$ value indicates a more effective IM.

2.2.2 Practicality

The criterion of practicality assesses the correlation between D_{max} and the IM. This is determined by the regression coefficient b, as shown in Eq. 3, which represents the slope of the linear regression between D_{max} and IM. A higher b value indicates a more practical IM.

2.2.3 Proficiency

The proficiency of an optimal IM is evaluated using ζ, which is the ratio of $\beta_{\mathrm{D|IM}}$ to b. This criterion provides a composite assessment of both practicality and efficiency. A lower ζ value signifies a more proficient IM.

2.2.4 Sufficiency

The sufficiency criterion (denoted by p-values) evaluates the conditional statistical independence of an IM from the magnitude (M_{w}) and closest distance like a Joyner-Boore

distance (R_{JB}) of earthquake events for the suite of ground motions (Padgett et al. 2007). In this study, the p-values are obtained by performing a linear regression of PSDM residuals ($\epsilon^{EDP}|IM$). The relationship of ($\epsilon^{EDP}|IM$) with M_w in Eq. 5 and R_{JB} in Eq. 6 were applied to determine IM sufficiency:

$$\varepsilon^{\mathrm{EDP}}|\mathrm{IM} = a_{\mathrm{M}} + b_{\mathrm{M}}\left(M_{\mathrm{w}}\right) \tag{5}$$

$$\varepsilon^{\mathrm{EDP}}|IM = a_{\mathrm{R}} + b_{\mathrm{R}}\left(R_{\mathrm{JB}}\right) \tag{6}$$

where a_M, b_M, a_R, and b_R are the regression coefficients. A more sufficient IM has higher p-values.

3 Ground Motion

This section provides an overview of ground motion characteristics relevant to seismic analysis in slope model simulation, focusing on the description of two sets of employed motion—horizontal only direction (set H), and horizontal and vertical combination (set HV). We then discuss the selected 19 IMs of ground motion used for optimal IM investigation.

3.1 Characteristics of Ground Motion

The nonlinear dynamic time history analysis of slopes used ground motions from a subset of Next Generation Attenuation West2 (NGA-West2) recordings. This subset contains 450 ground motion records from 137 stations and 61 earthquake events. For reliable PSDMs, this collection of 450 ground motion records from varied seismic sources, sites, magnitude, and distance is sufficient. According to the Applied Technology Council (ATC-63) (Deierlein et al. (2008), the ground motions were selected to ensure that they have the potential to induce structural collapse. These ground motions meet criteria related to earthquake magnitude, recording conditions, and diversity, with no more than two records from a single event to reduce bias. Previous research has demonstrated that well-distributed datasets of this size can reduce statistical bias and ensure stable regression in fragility and demand modeling. For example, Baker (2015) discussed the use of regression-based methods in ground motion selection and indicated that hundreds of records are generally adequate for stable PSDM. Shome et al. (1998), Cornell (1999), Mackie and Stojadinovic (2001), and McCartney et al. (2020) suggested that 100–300 ground motions may be sufficient for fragility analysis if well-distributed across IMs and source to site distance characteristics. Tothong and Luco (2007) also highlighted that model stability in PSDM improves with growing diversity of records, rather than simply increasing the number of records. Among the 450 ground motion records: 150 are in horizontal direction 1 (H1), 150 are in horizontal direction 2 (H2), and 150 are vertical (V) records. Each H1 and H2 record was paired with a vertical component, resulting in 300 combined horizontal-vertical motion (150 H1+V and 150 H2+V). For the analysis, we considered two main sets: Set H, including 300 horizontal motions (150 H1 and 150 H2), and Set HV, comprising the 300 combined horizontal-vertical pairs. This dataset configuration allows for a comprehensive evaluation of seismic effects across different component combinations. Normally, vertical ground motion is usually minor compared to horizontal motions. Eurocode 8 (EU 2004) proposed that vertical accelerations are 70% of horizontal ones. Combining vertical and horizontal components increases their impact on seismic demand and structural response (Murthy and Patil 2015; Wibowo and Sritharan 2022; Wang et al. 2023). Thus, using horizontal-only and horizontal-vertical inputs enables for a more relevant and thorough seismic effect assessment, which is a standard seismic analysis technique. As a result, this dataset is sufficient to minimize statistically biased estimation in the PSDM. Figure 1 illustrates the spectral acceleration (5% damped) of the selected ground motions. H1 represents higher PGA (from 0.01 to 1.4 g) at a station for a specific earthquake event than H2 (from 0.0088 to 1.26 g). The vertical components exhibit the lowest PGA values,

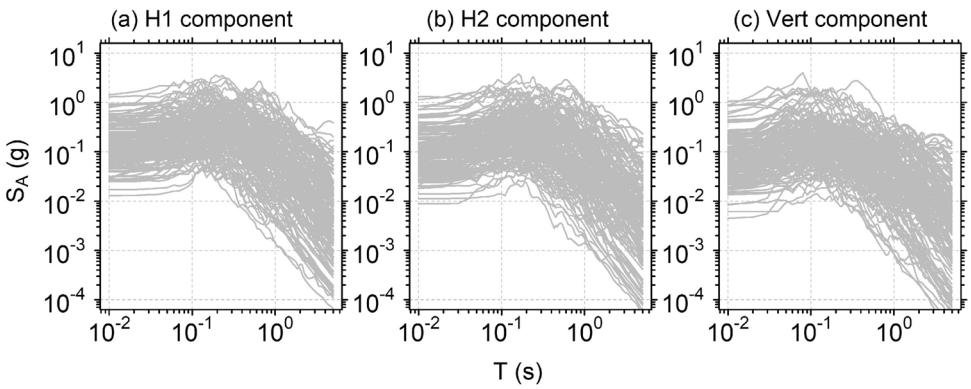

Fig. 1 Spectral acceleration (5% damped) of selected ground motions: **a** H1, **b** H2, and **c** the vertical component

ranging from 0.0046 to 1.23 g. Two distinct sets of input motions were created to evaluate the impact of the vertical ground motion on the seismic fragility of slopes.

3.2 Selected Intensity Measures (IMs) of Ground Motion

To find the most effective indicators for the PSDM of slope, we examined a total of 19 IMs. These IMs were selected based on the criteria derived from prior studies (Tothong and Luco 2007; Hariri-Ardebili and Saouma 2016; Nguyen, Shin, et al. 2023). Specifically, the selection framework included three key requirements: (1) relevance to geotechnical and slope stability applications, as opposed to structural-only IMs; (2) comprehensive coverage of major IM categories, such as peak-based (for example, PGA, PGV), energy-based (for example, I_A, CAV), frequency content (for example, dominant frequency - f_{max}), duration-related, and spectral-based measures (for example, ASI, VSI, HI); and (3) useful in slope or geotechnical demand investigations. For all 19 IMs, horizontal values are consistently greater than vertical values. Additionally, within the horizontal measures, H1 exhibits higher values than H2. In the approach suggested by Hariri-Ardebili and Saouma (2016), the selected IMs were categorized into two groups: ground motion-dependent scalar IMs (Group 1) and structure-dependent spectral IMs (Group 2). Group 1 encompasses 15 parameters, including:

Peak ground acceleration (PGA),

$$\mathrm{PAG} = \max|a(t)|, (g) \text{ (Trifunac and Brady 1975);} \tag{7}$$

Peak ground velocity (PGV),

$$\mathrm{PGV} = \max|v(t)|, (\mathrm{m/s}) \text{(Trifunac and Brady 1975);} \tag{8}$$

Peak ground displacement (PGD),

$$\mathrm{PGD} = \max|d(t)|, (\mathrm{m}) \text{(Trifunac and Brady 1975);} \tag{9}$$

Ratio of PGV/PGA (Malhotra 1999);

Root-mean-square of acceleration (a_{RMS}),

$$a_{\mathrm{RMS}} = \sqrt{\frac{1}{t_{\mathrm{total}}}\int_0^{t_{\mathrm{total}}}(a(t))^2dt}, (\mathrm{g}) \text{ (Kramer 1996);} \tag{10}$$

Root-mean-square of velocity (v_{RMS}),

$$v_{\mathrm{RMS}} = \sqrt{\frac{1}{t_{\mathrm{total}}}\int_0^{t_{\mathrm{total}}}(v(t))^2dt}, \ (\mathrm{m/s}) \text{(Housner 1975);} \tag{11}$$

Root-mean-square of displacement (d_{RMS}),

$$d_{\mathrm{RMS}} = \sqrt{\frac{1}{t_{\mathrm{total}}}\int_0^{t_{\mathrm{total}}}(d(t))^2dt}, (\mathrm{m}) \text{(Riddell and Garcia 2001);} \tag{12}$$

Arias intensity (I_A),

$$I_{\mathrm{A}} = \frac{\pi}{2g}\int_0^{t_{\mathrm{total}}}(a(t))^2dt, (\mathrm{m/s}) \text{(Arias 1970);} \tag{13}$$

Characteristic intensity (I_C),

$$I_{\mathrm{C}} = \left(a_{\mathrm{RMS}}\right)^{3/2}\sqrt{t_{\mathrm{total}}}, \text{(Park et al.1985);} \tag{14}$$

Specific energy density (SED),

$$\mathrm{SED} = \int_0^{t_{\mathrm{total}}}(v(t))^2dt, \ (\mathrm{m^2/s}) \text{ (Kramer 1996)} \tag{15}$$

Cumulative absolute velocity (CAV),

$$\mathrm{CAV} = \int_0^{t_{\mathrm{total}}}|a(t)|dt, \ (\mathrm{m/s}) \text{(Reed and Kassawara 1990);} \tag{16}$$

Cumulative absolute displacement (CAD),

$$\mathrm{CAD} = \int_0^{t_{\mathrm{total}}}|v(t)|dt, (\mathrm{m}) \text{(Mackie and Stojadinovic 2001);} \tag{17}$$

Sustained maximum acceleration (SMA),

SMA = 3rd highest absolute value of acceleration time history, (g) (Nuttli 1979);

Sustained maximum velocity (SMV),

SMV = 3rd highest absolute value of velocity time history, (m/s) (Nuttli 1979);

and Dominant frequency (f_{max}),

f_{max} = maximum Fourier amplitude in Fourier spectra, (Hz) (Kramer 1996).

Group 2 includes four parameters—acceleration spectrum intensity, velocity spectrum intensity, Housner intensity, and effective peak acceleration. The selection of these four IMs was based on their extensive use in previous studies (Padgett et al. 2007; Che et al. 2023). Their broad use and performance evaluation efficacy make them ideal for our investigation.

Acceleration spectrum intensity (ASI),

$$\mathrm{ASI} = \int_{0.1}^{0.5} S_a(\zeta = 5\%, T)dT, (\mathrm{g \cdot s}) \text{(Thun et al.1988);} \tag{18}$$

Velocity spectrum intensity (VSI),

$$\mathrm{VSI} = \int_{0.1}^{2.5} S_v(\zeta = 5\%, T)dT, \ (\mathrm{m}) \text{(Thun et al.1988);} \tag{19}$$

Housner intensity (HI),

$$\mathrm{HI} = \int_{0.1}^{2.5} PS_v(\zeta = 5\%, T)dT, (\mathrm{m})(\text{Housner 1975}); \quad (20)$$

and effective peak acceleration (EPA),

$$\mathrm{EPA} = \frac{\mathrm{mean}\left(S_a^{0.1-0.5}(\zeta = 5\%)\right)}{2.5}, (\mathrm{g})(\text{Kurama and Farrow 2003}). \quad (21)$$

4 Model Set-Up

The nonlinear time history analyses of slopes were performed using the PLAXIS-2D software (Bentley 2022) to compute $D_{\max}$ based on the PLAXIS-Material guidelines in 2024 (Bentley 2024). Some research suggested that seismic slope stability analysis should consider slope heights between 5 and 30 m (Pushpa et al. 2016; Kumar et al. 2023; Meko et al. 2023). In seismically active areas, various natural and human-made slopes must be assessed for static and dynamic stability. Effective slope stability assessments require knowing the influence of slope height within this range (for example, 10 m, 20 m, and 30 m). As shown in Fig. 2, in the models at $H_{\text{slope}} = 20$ m, and 30 m, the slope part was divided into 10 m sublayers to account for confinement's effect on the soil's nonlinear curves. Additionally, constant inclination (β) of 30° and a 10 m foundation soil layer is maintained. The current analysis ignores the geometric features in slope deformation, even though it fixes the slope inclination at $\beta = 30°$. The method works well for preliminary slope stability studies. Finally, three models at H_{slope} of 10, 20, and 30 m at $\beta = 30°$ were created and subjected to sets H and HV ground motion in simulations. Table 1 shows the geometries of these models.

This study examined one soil type. The soil's strength was assessed using the Mohr-Coulomb failure criterion, which considers c and ϕ. Soil stiffness was determined by shear wave velocity (V_S). Table 2 lists the soil properties of slope models. The HS-small model (Bentley 2024) was used to evaluate soil behavior under cyclic loading. This material model allows for soil nonlinearity and hysteresis energy dissipation. The HS-small model requires nonlinear

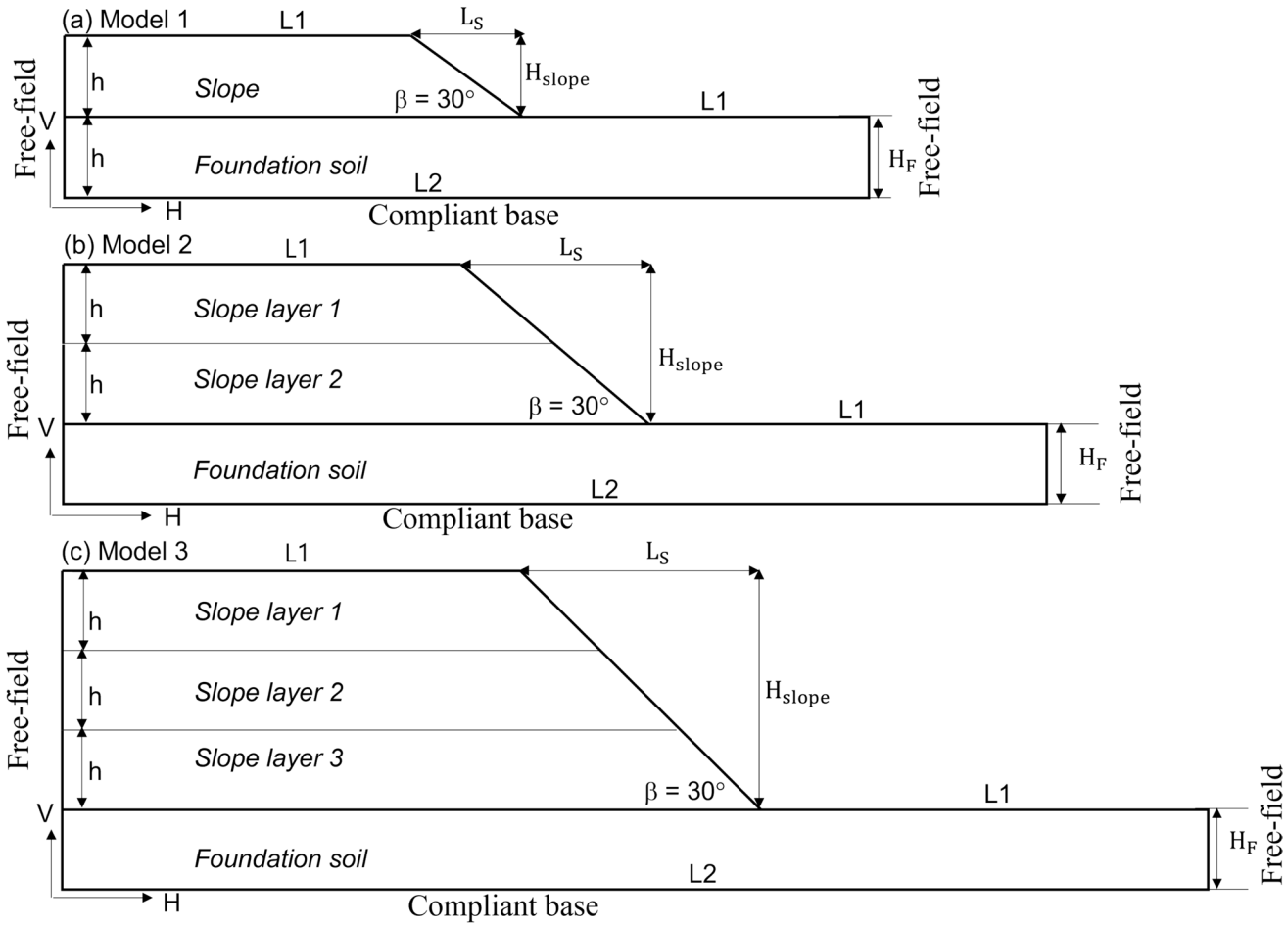

Fig. 2 Three slope models with $\beta = 30°$ and a foundation of 10 m thick: H_{slope}= **a** 10 m; **b** 20 m; and **c** 30 m

Table 1 Configuration parameters of the three models in this study

Model No.	H_{slope}(m)	$L1$ (m)	$L2$ (m)	L_S(m)	H_F(m)	h (m)
1	10	45.1	107.5	17.3	10	10
2	20	90.15	215	34.6	10	10
3	30	135.2	322.4	52	10	10

Table 2 Material properties of the three models

Model	Slope component	V_S(m/s)	Cohesion c (kPa)	Friction angle ϕ (°)
1, 2, 3	Slope layers in H_{slope}	200	10	30
	Foundation soil	300	10	35

soil curves (that is, modulus reduction (G/G_{max}) and damping ratio). Thus, we used the empirical model from Stokoe, II et al. (2001). The Rayleigh damping models soil damping from 0.55% to 0.98% using two frequencies: f1 (based on system fundamental frequency) = V_S/(4×H), where H is the model height ($H = H_{slope} + H_F$); and the second frequency f2 (5 × f1), as proposed by Kwok et al. (2007). We used a 15-node triangular element with a high mesh density for accuracy.

The simulations employed Cundall et al.'s (1980) free-field conditions for the lateral side boundaries and Lysmer and Kuhlemeyer's (1969) compliant base for bottom in PLAXIS-2D. The lateral sides and bottom of the slope models were protected from intentionally reflected waves by these boundary conditions. A viscous dashpot system accommodates horizontal and vertical seismic movements in the compliant boundary condition. Equations 22 and 23 integrate the acceleration time series of the ground motions for the horizontal and vertical components into velocity time series to calculate shear and normal stresses for this system:

$$\tau(t) = V_{S,base} \times \rho_{base} \times \dot{u}_h(t) \tag{22}$$

$$\sigma(t) = V_{P,base} \times \rho_{base} \times \dot{u}_v(t) \tag{23}$$

where $\tau(t)$ presents the time history of shear stress at the slope model base, ρ_{base} is the density of the model, that is, 1800 kg/m^3 for slope, and 2000 kg/m^3 for foundation soil. $V_{S,base}$ is the shear wave velocity, the value of 300 m/s is set for foundation. $\dot{u}_h(t)$ is the velocity time series of the ground motions for the H1 and H2 components. $\sigma(t)$ is the time history of normal stress at the model base. $V_{P,base}$ is the compressional wave velocity of the model base ($V_{P,base}$ = 489.3 m/s for foundation). $\dot{u}_v(t)$ is the velocity time series of the vertical component.

We compared our model's D_{max} to other research using PLAXIS-2D and FLAC-2D to verify slope nonlinear time history (Latha and Garaga 2010; Zhang et al. 2012; Özmen 2019). Previous studies' ground motions were employed for all three slopes. Parameters, and free-field and compliant base boundary conditions, were taken from prior studies. The D_{max} calculated in this study are identical to those from the mentioned research during the full length. The D_{max} obtained at the end of the ground motion is less than 4% different from the previous investigations. We also evaluated R^2 values for displacement time series disparities between our results and previous studies. R^2 = 0.97, 0.88, and 0.98 for Özmen (2019), Latha and Garaga (2010), and Zhang et al. (2012) analyses, respectively. These values are near 1.0, indicating good slope modeling. To further verify the numerical results, we compared the simulated permanent displacement with those computed using the Newmark sliding block method. The discrepancy (≈ 14%) indicates good agreement and supports the reliability of the adopted modeling framework.

5 Optimal Intensity Measure (IM) Considering D_{max}

This section identifies the optimal IM by evaluating the EDP of slopes in PSDM. This study evaluated seismic slope performance using D_{max} as the major EDP. Displacement-based criteria are widely used in geotechnical earthquake engineering to estimate slope collapse potential more realistically and practically than factors of safety. D_{max} directly measures irreversible deformation under seismic action, which is crucial for slope serviceability and post-earthquake functionality. Travasarou and Bray (2003), Crowley (2004), Rathje and Saygili (2009), and Fotopoulou and Pitilakis (2015) have used displacement-based EDPs to create seismic demand models. The slopes were subjected to sets H and HV to determine D_{max}. Figures 3 and 4 illustrate the distribution of D_{max} against 19 IMs of set H and HV at three slope heights. Seismic displacements rise with slope height due to gravity. The D_{max} of slopes increases with the rise in slope height.

5.1 Subjected to the Horizontal Ground Motion

This section focuses on identifying the optimal IM for evaluating D_{max} under set H. Section 5.1.1 examines the results of efficiency, practicality, and proficiency. Section 5.1.2

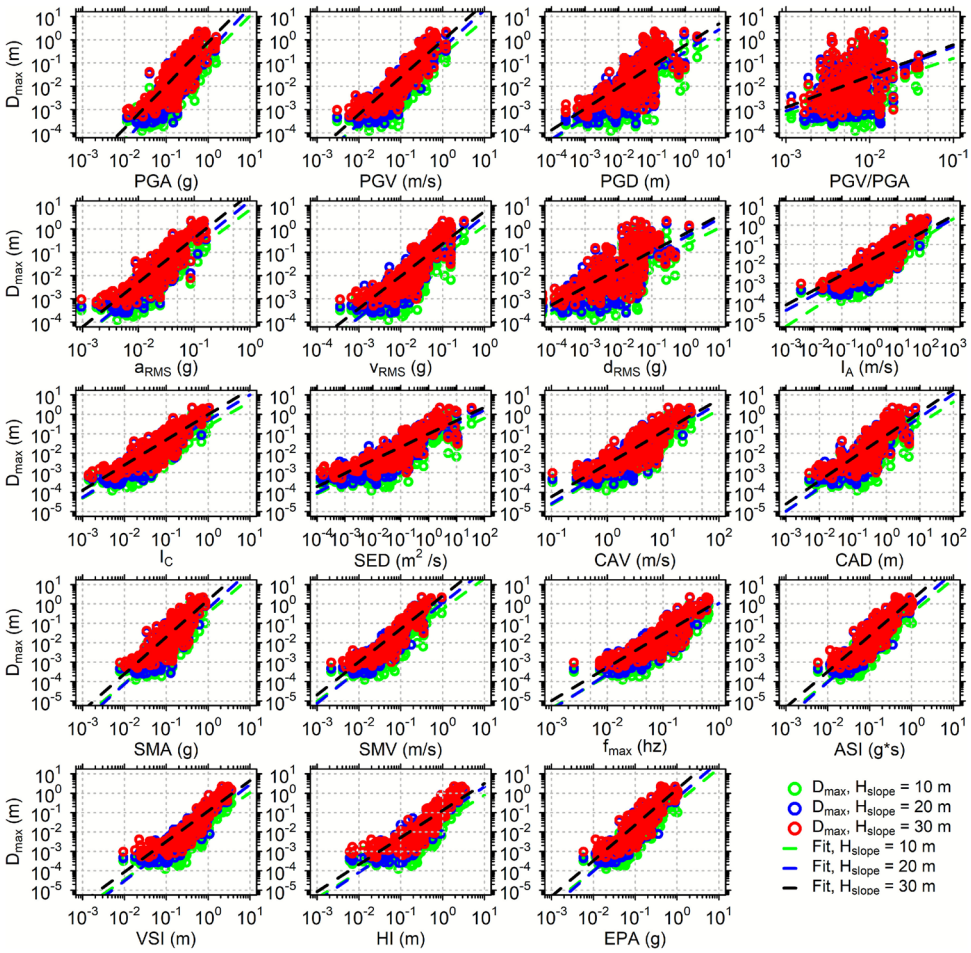

Fig. 3 Distribution of D_{max} against 19 intensity measures (IMs) computed for set H

addresses the criterion of sufficiency, confirming the selected IM comprehensively.

5.1.1 Efficiency, Practicality, and Proficiency

$\beta_{D|IM}$ Evaluates the efficiency of IMs, and as explained in Sect. 2.2, lower $\beta_{D|IM}$ indicates greater effectiveness. To align with other criteria that higher values indicate greater IM efficiency, we consider the inverse value of $\beta_{D|IM}$ (that is, $1/\beta_{D|IM}$). The obtained $1/\beta_{D|IM}$ for IMs across the three models are presented in Fig. 5. The IM of I_A is identified as the most efficient for the slope at 10 m of height, where $1/\beta_{D|IM} = 1.035$. Following I_A, f_{max} and I_C show high efficiency at $1/\beta_{D|IM} = 1.031$ and 1.027, respectively. For the slopes with heights of 20 m and 30 m, the most efficient IMs shift to VSI ($1/\beta_{D|IM} = 1.078$ and 1.094, respectively), followed by SMV and PGV ($1/\beta_{D|IM} = 1.077$ and 1.083 for heights of 20 m and 30 m). The results demonstrate that IMs related to acceleration time history (for example, I_A, I_C, ASI, EPA) are more efficient for the 10 m slope. Additionally, velocity-related IMs (for example, PGV, SMV, and VSI) contribute significantly to the efficiency for this model. Conversely, for medium-height and higher slopes (20 m and 30 m, respectively), velocity-related IMs (for example, VSI, SMV, and PGV) exhibit greater efficiency. Acceleration-related IMs (for example, ASI, EPA, I_A, and I_C), also show appreciable efficiency. f_{max}, related to dominant frequency, shows high efficiency across all three models, with $1/\beta_{D|IM} = 1.031$, 0.99, and 1.038, respectively. In contrast, displacement-based IMs (PGD, RMS, and CAD) are relatively less efficient across the three slope heights.

Figure 6 presents the practicalities of the IMs via computed b values. The figure shows that SMA achieves the highest b across three slope heights ($b = 1.82$, 2.04, and 1.805 for heights of 10 m, 20 m, and 30 m, respectively). Following SMA, a_{RMS} and PGA exhibit higher b values. Specifically, for a_{RMS}, $b = 1.80$, 2.03, and 1.802 for the respective heights of 10 m, 20 m, and 30 m, while for PGA, $b = 1.77$, 2.01, and 1.76 for the same heights. Generally, acceleration-related IMs (for example, SMA, a_{RMS}, PGA, ASI, EPA, and CAV) demonstrate greater practicality across the three slopes compared to others. Displacement-related IMs (for example, RMSD, PGD, CAD, and SED) exhibit lower b, indicating relatively less practicality.

To determine proficiency, we consider the criteria of ζ. The inverse value of ζ is applied for consistent tendency

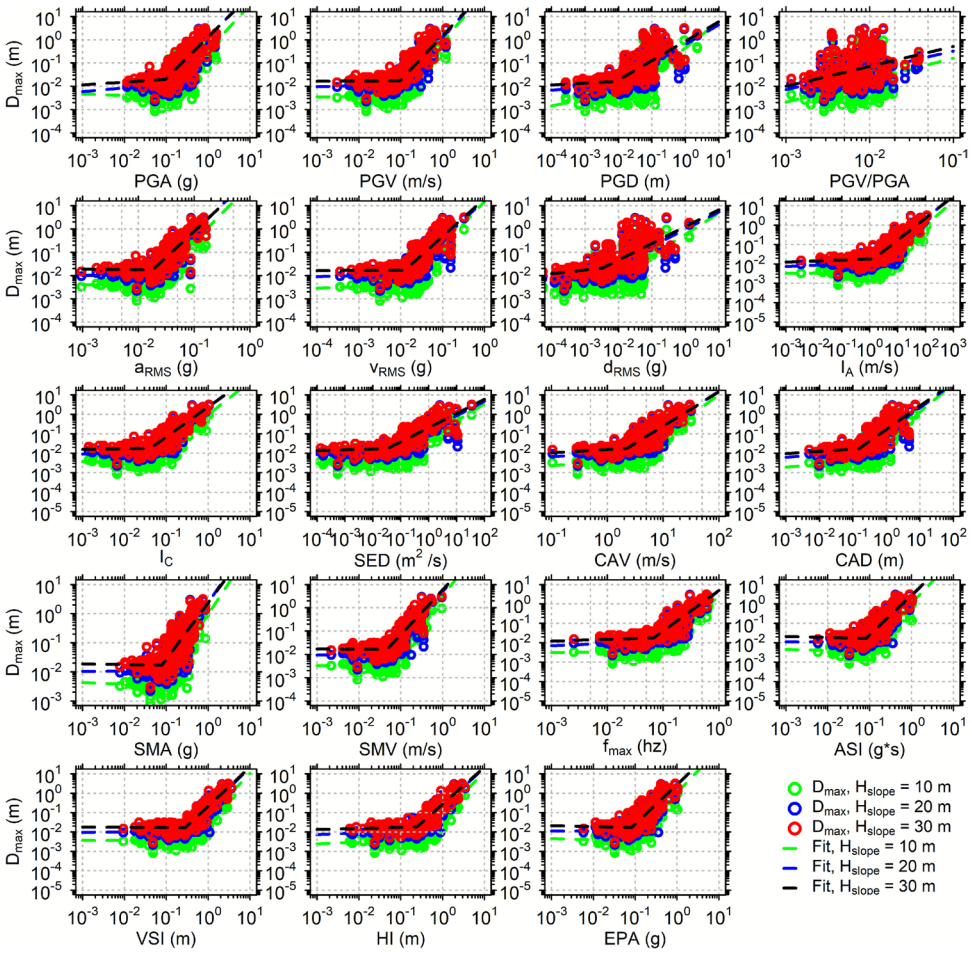

Fig. 4 Distribution of D_{max} against 19 intensity measures (IMs) computed for set HV

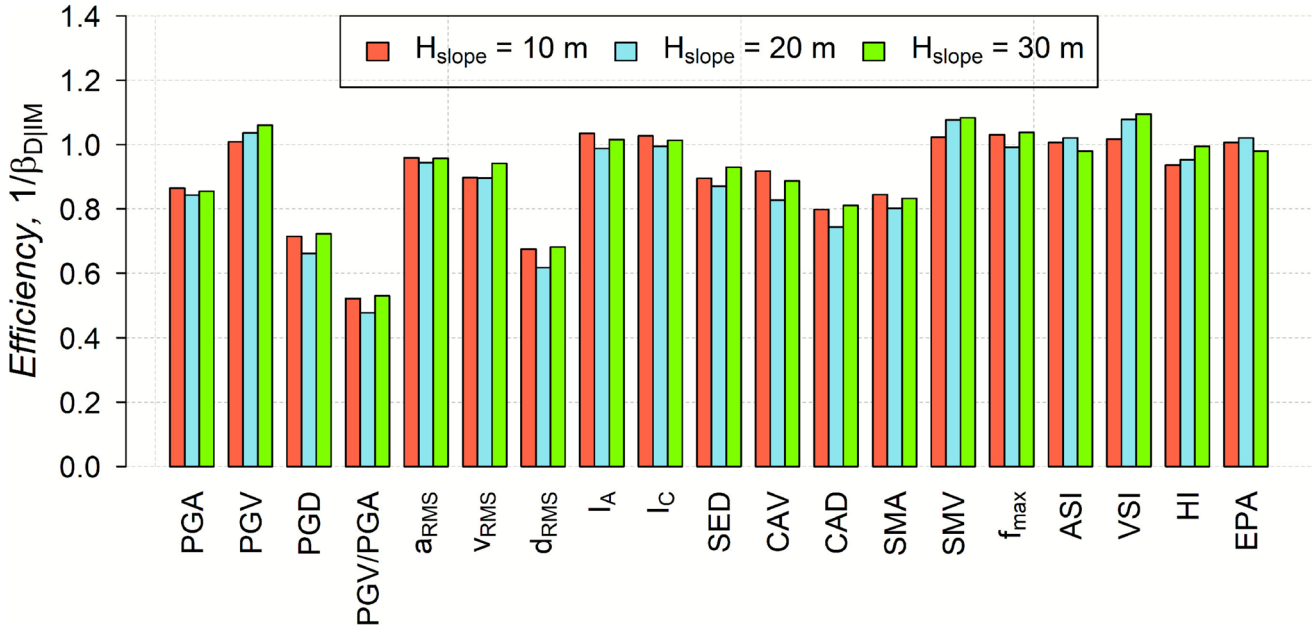

Fig. 5 $1/\beta_{D|IM}$ for intensity measures (IMs) in the three models subjected to set H

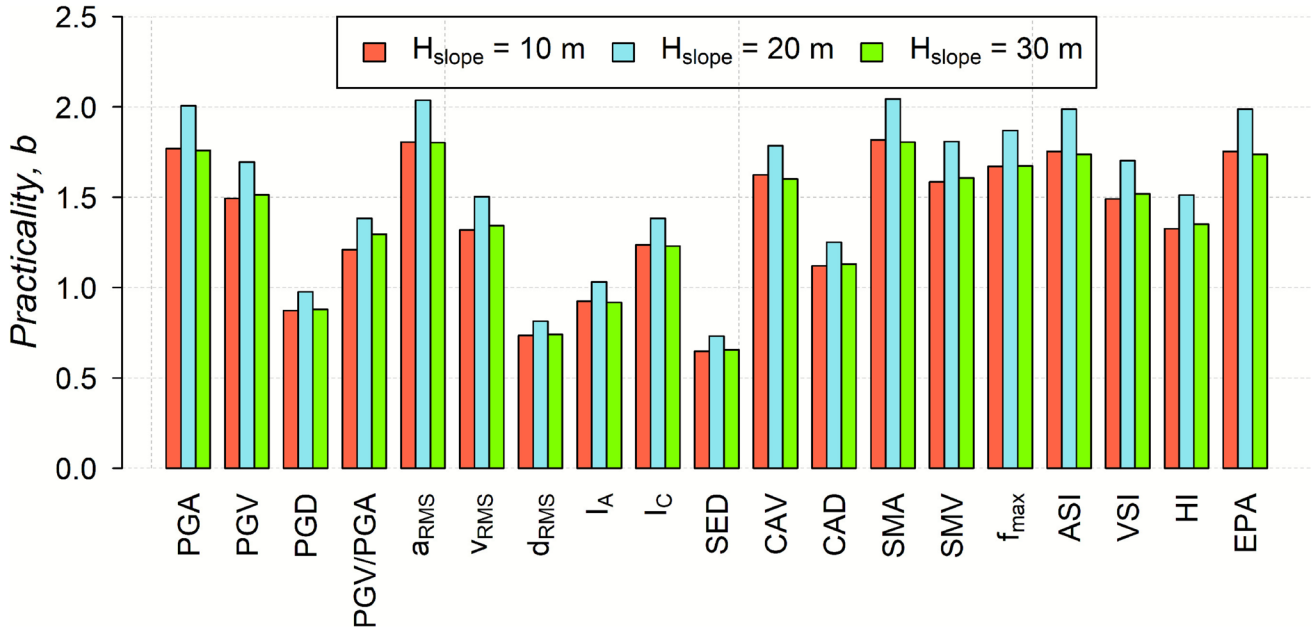

Fig. 6 b values for intensity measures (IMs) in the three models subjected to set H

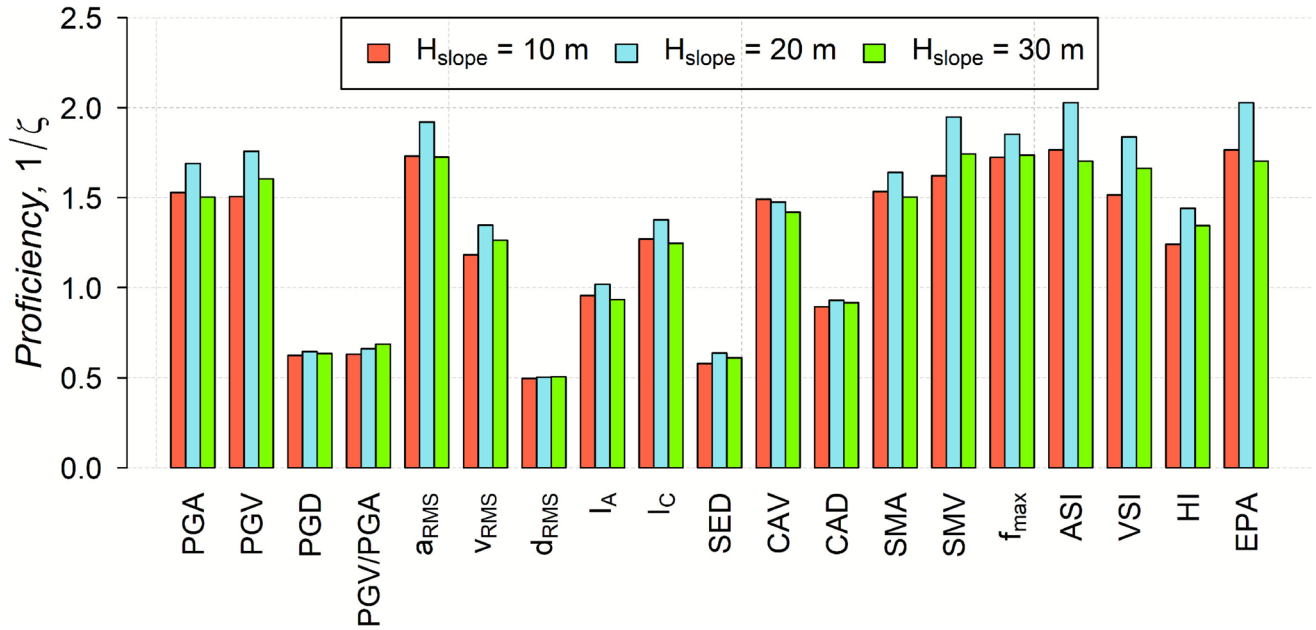

Fig. 7 $1/\zeta$ values for intensity measures (IMs) in the three models subjected to set H

with the other parameters—higher $1/\zeta$ indicates a higher proficiency. The computed $1/\zeta$ are shown in Fig. 7. For lower slopes (H_{slope} = 10 m and 20 m), ASI ($1/\zeta_{\text{ASI}}$ = 1.77 and 2.03 corresponding to H_{slope} = 10 m and 20 m, respectively) tends to be the most proficient. Following ASI, two IMs of EPA ($1/\zeta_{\text{EPA}}$ = 1.76 for H_{slope} = 10 m, and 2.02 for H_{slope} = 20 m) and a_{RMS} ($1/\zeta_{a_{\text{RMS}}}$ = 1.73 and 1.93 for H_{slope} = 10 m and 20 m, respectively) show more proficiency. These numbers imply that the parameter related to displacement time history exhibits the highest proficiency. For the model of 30 m, SMV shows the highest proficiency with $1/\zeta_{\text{SMV}}$ = 1.74, followed by f_{max} ($1/\zeta_{f_{\text{max}}}$ = 1.73) and a_{RMS} ($1/\zeta_{a_{\text{RMS}}}$ = 1.72). Displacement-based IMs (for

example, d_{RMS}, SED, and PGD) and PGV/PGA are less proficient in all models.

5.1.2 Sufficiency

The sufficiency of the IMs relative to M_w and R_{JB} is illustrated in Figs. 8 and 9, respectively. For M_w, SMA and PGV/PGA are identified as the most sufficient. Specifically, SMA is the most sufficient at lower slopes of 10 m and 20 m, while PGV/PGA is most sufficient for the slope of 30 m. For R_{JB}, SMA remains the most sufficient for the lower slopes, whereas PGA shows the highest sufficiency for the model of 30 m. These results confirm that the most sufficient IMs related to distance and magnitude

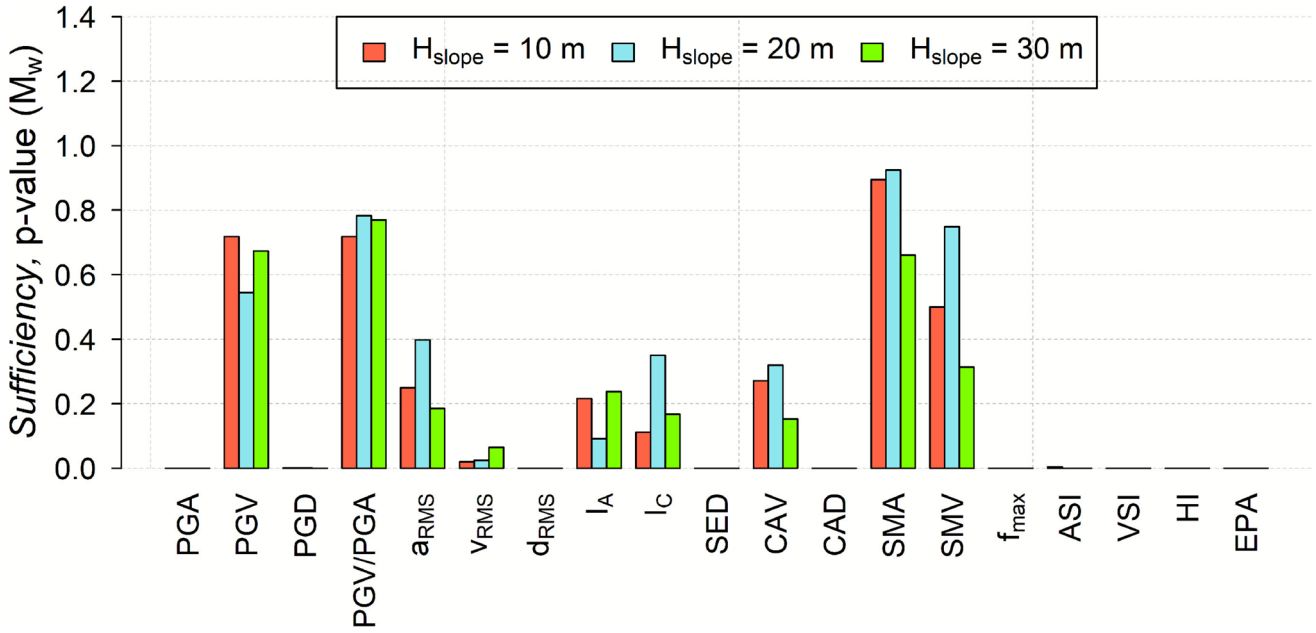

Fig. 8 *P*-values considering M_w in the three models subjected to set H

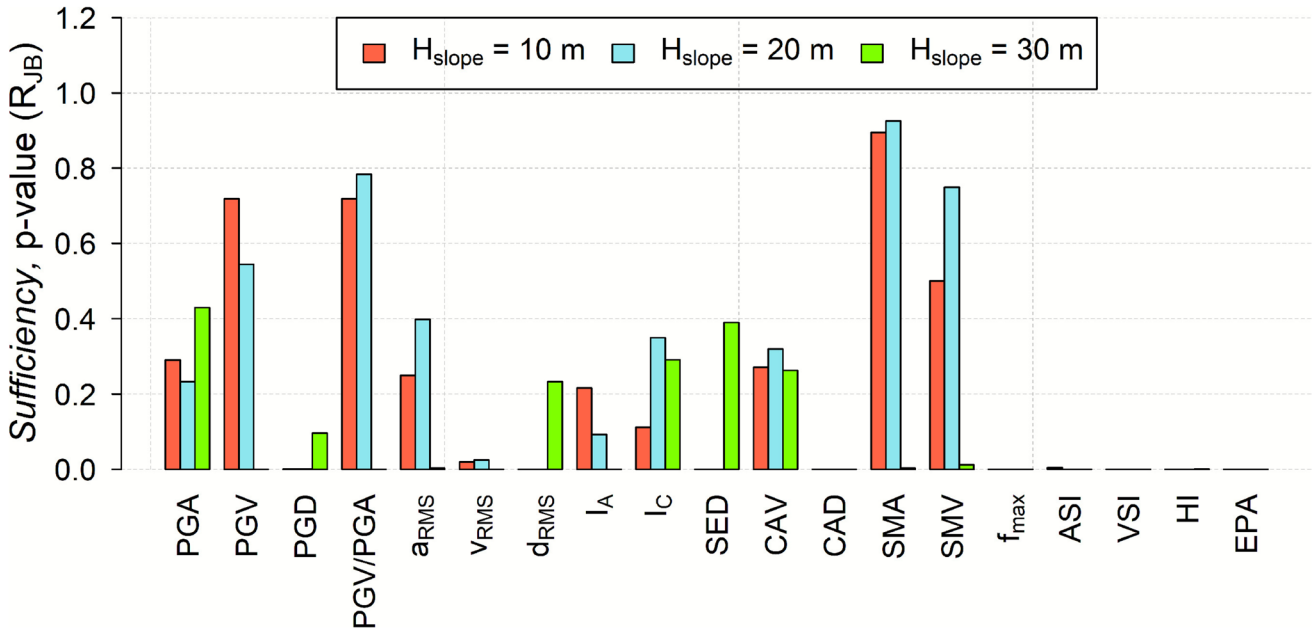

Fig. 9 *P*-values considering R_{JB} in the three models subjected to set H

are consistent for lower slopes but differ for the highest model.

5.1.3 Summary of the Results

The final ranking was derived by normalizing and combining the four criteria into a composite score, following the approach of Hariri-Ardebili and Saouma (2016). Table 3 shows the top three proposed IMs for slopes subject to set H based on four criteria. The ranking priority column shows IM weight in increasing optimization level. The results indicate that acceleration-related IMs (SMA, a_{RMS}, and PGA) and velocity-related IMs (VSI, PGV, and SMV) are optimal for these slopes. For lower slopes (10 m and 20 m), acceleration-related IMs are predominant, while the velocity-related SMV emerges as the key parameter for the highest slope (30 m). According to the priority ranking, SMA is recommended as the optimal IM for the lower and medium-height slopes of 10 m and 20 m, whereas SMV is suggested as the optimal IM for the highest model of 30 m.

Table 3 Optimal intensity measures (IMs) for the three slope models subjected to set *H*

For set *H* motions	Priority ranking	Slope height		
		10 m	20 m	30 m
IMs	1	SMA	SMA	SMV
	2	a_{RMS}	PGV	SMA
	3	f_{max}	SMV	a_{RMS}

5.2 Subjected to the Set HV Motions

This subsection determines the optimal IM for evaluating D_{max} under set HV. Section 5.2.1 evaluates three criteria: efficiency, practicality, and proficiency. Section 5.2.2 assesses sufficiency, confirming the selected IM comprehensively.

5.2.1 Efficiency, Practicality, and Proficiency

Figure 10 provides values of $1/\beta_{D|IM}$ for 19 IMs in the three models. The IM of PGV is the most efficient for the lowest and highest models (H_{slope} = 10 m and 30 m), while I_A shows highest $1/\beta_{D|IM}$ for the medium model of 20 m. It implies that the IM related to velocity achieves higher efficiency than others on the lowest and highest models under the effect of vertical motion. Acceleration-based parameter contributes to higher efficiency than others for a medium model. Conversely, the IMs related to displacement (for example, CAD and SED) present less efficiency for the three slopes. This result is consistent with cases subjected to set H.

Figure 11 illustrates practicality through *b*, where SMA is identified as the most practical across the three models. The IMs of PGA and a_{RMS} show high practicality. Conversely, IMs related to displacement are less practical. These findings are similar to the results of models subjected to set H.

Figure 12 displays proficiency through $1/\zeta$ values. a_{RMS} is the most proficient IM across the three models, followed by PGA and PGV, implying that acceleration-based parameters from HV demonstrate significant proficiency compared to others. On the other hand, SED, related to displacement,

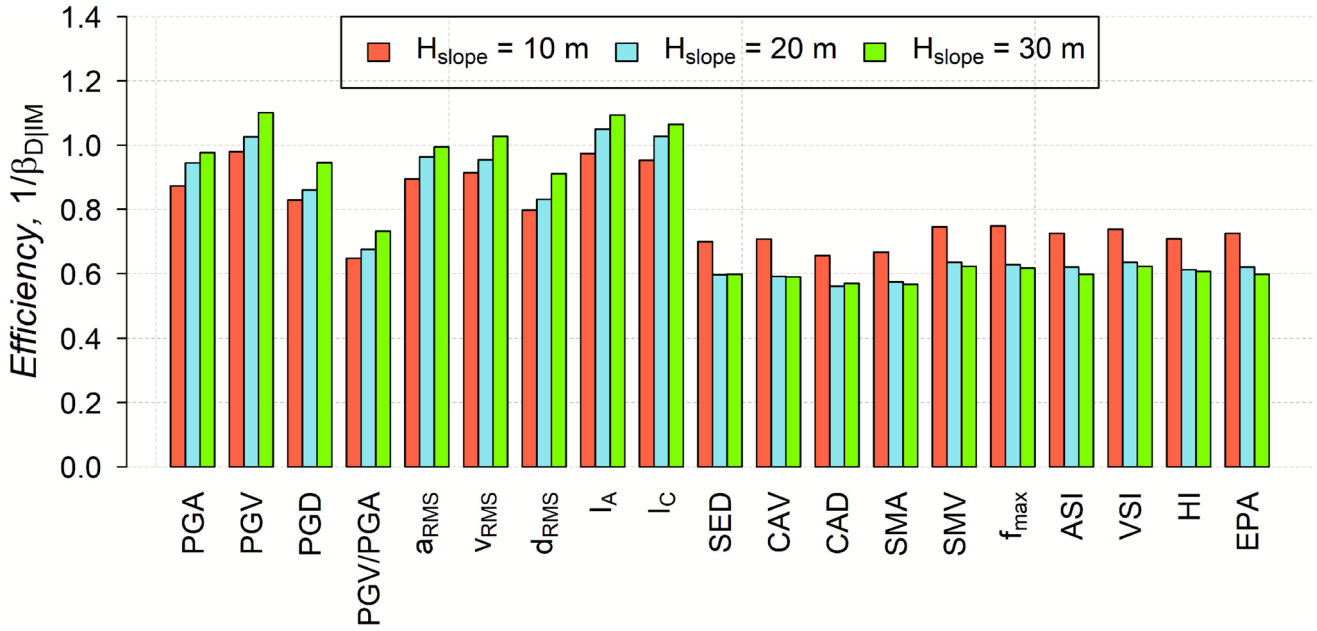

Fig. 10 $1/\beta_{D|IM}$ for intensity measures (IMs) in the three models subjected to set HV

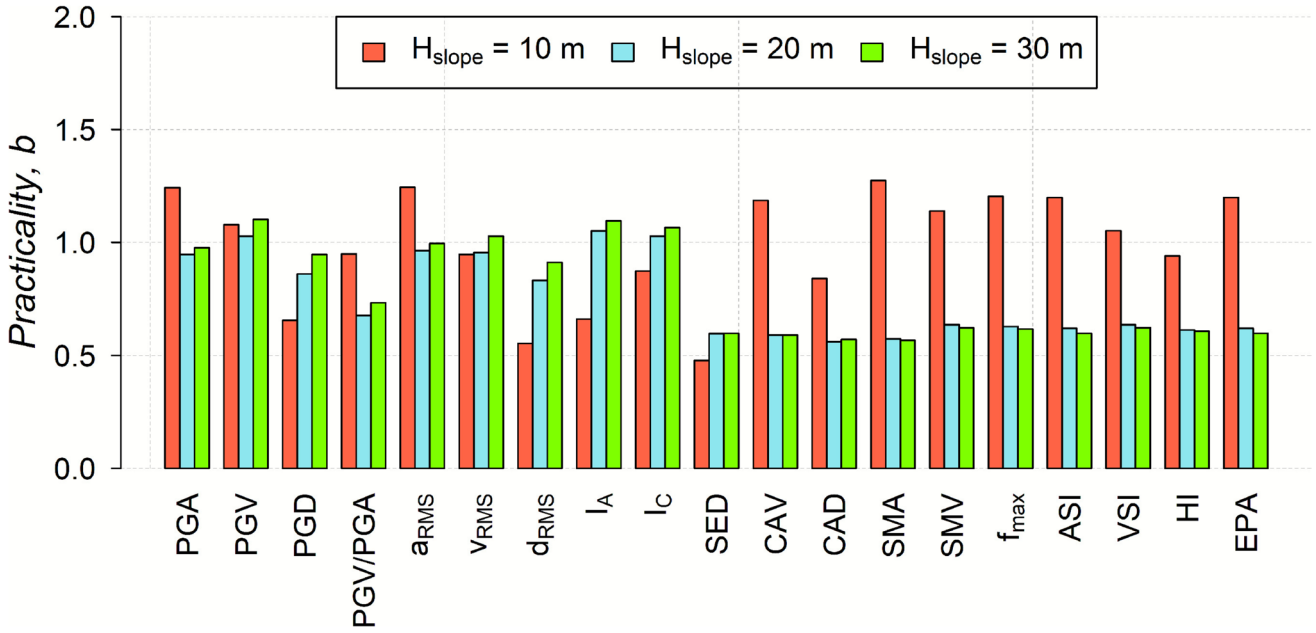

Fig. 11 *b* values for intensity measures (IMs) in the three models subjected to set HV

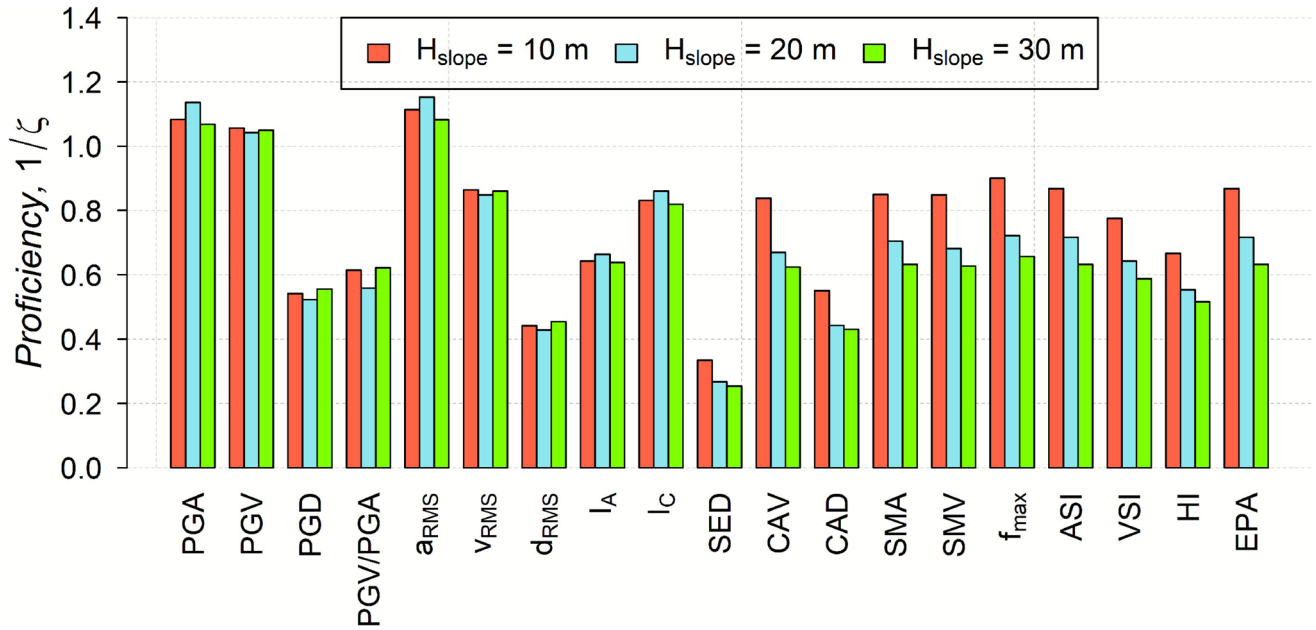

Fig. 12 $1/\zeta$ for intensity measures (IMs) in the three models subjected to set HV

shows negligible proficiency, consistent with findings from models subjected to set H.

5.2.2 Sufficiency

Figures 13 and 14 illustrate the sufficiency of IMs relative to M_w and R_{JB} for slopes subjected to set HV. For M_w, SMA and PGV/PGA are the most sufficient for the three models. Specifically, SMA is the most sufficient for the lowest and highest models of 10 m and 30 m, while PGV/PGA is optimal for the medium model of 20 m. Regarding R_{JB}, the IMs of SMA, PGV/PGA, and SED are the most sufficient for the models at 10 m, 20 m, and 30 m,

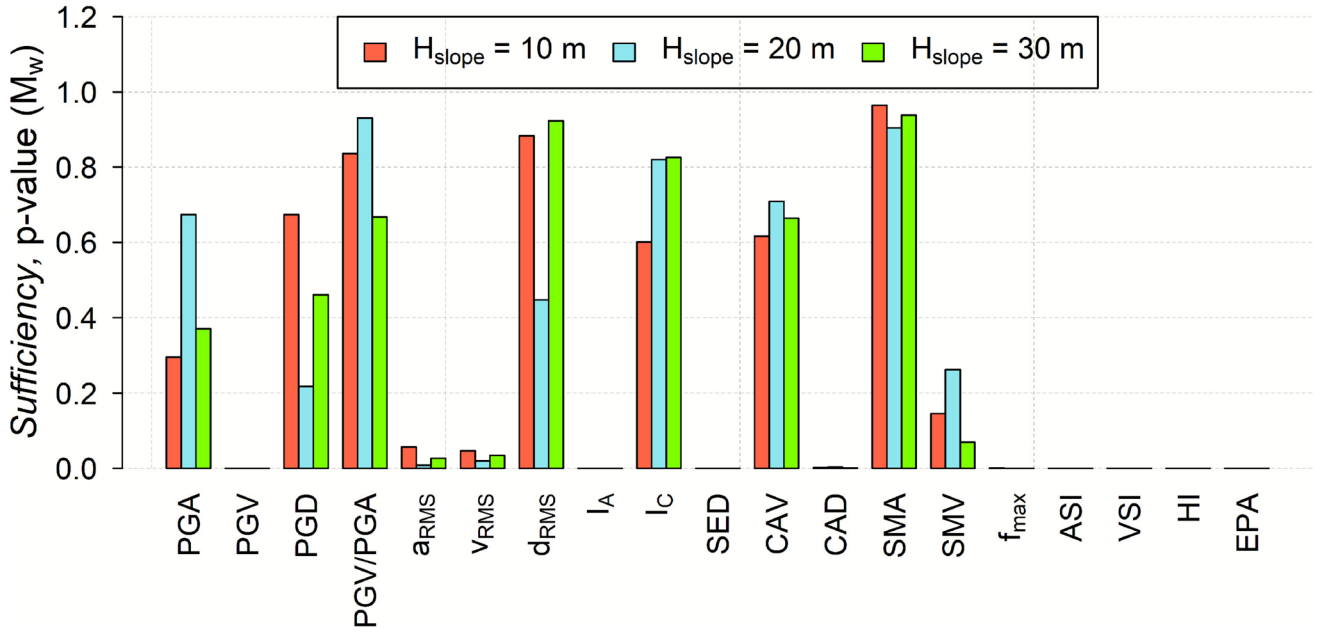

Fig. 13 *P*-values considering M_w in the three models subjected to set HV

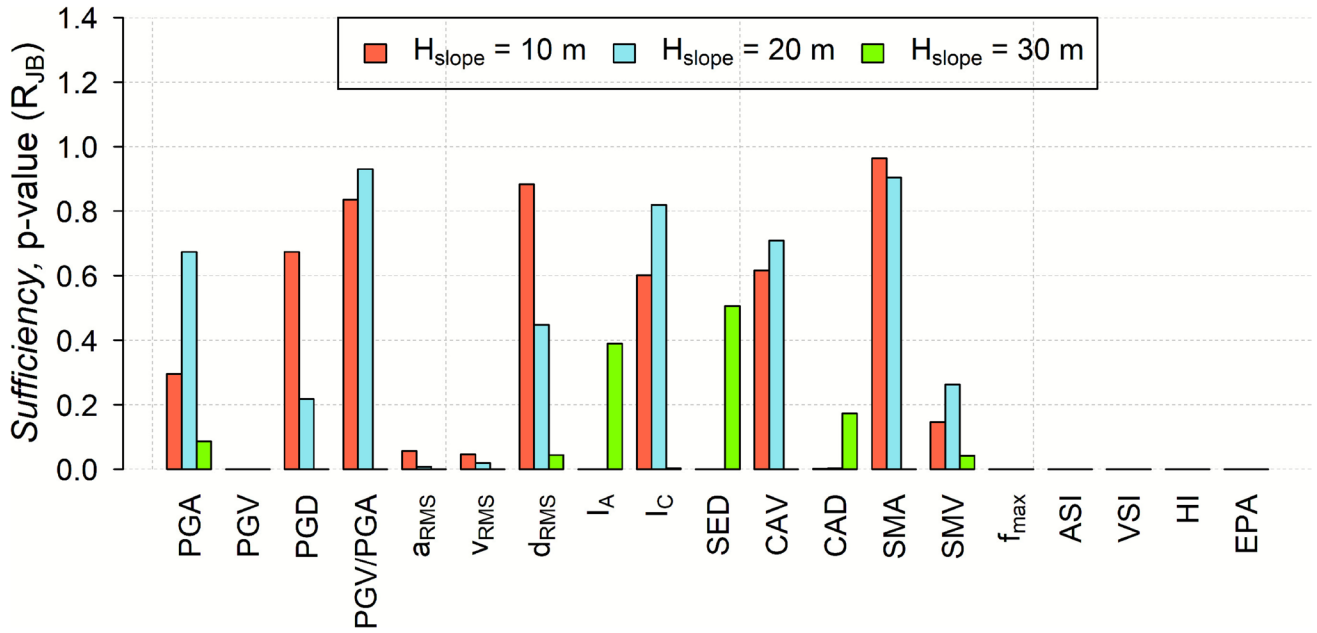

Fig. 14 *P*-values considering R_{JB} in the three models subjected to set HV

respectively. These results suggest that the most sufficient IMs related to M_w differ from those related to distance.

5.2.3 Summary of the Results

Table 4 lists the optimal IMs for the set HV in the three models. The acceleration-related IMs have dominant effect on D_{max}. The velocity-related IMs present a high effect. Based on the priority list, SMA is the optimal IM for the three models, and a_{RMS} is another good choice.

Table 4 Optimal intensity measures (IMs) for the three slope models subjected to set HV

For set HV motions	Priority ranking	Slope height		
		10 m	20 m	30 m
IMs	1	SMA	SMA	SMA
	2	PGA	a_{RMS}	a_{RMS}
	3	a_{RMS}	PGA	PGV

5.3 Probabilistic Seismic Demand Model (PSDM)-Based Fragility Assessment

Based on the PSDM approach presented in Sect. 2.1 and optimal IMs in Tables 3 and 4, fragility curves are generated for set H and HV as shown in Figs. 15 and 16, respectively. The fragility curves generated for D_{max} are used to quantify slope seismic vulnerability by considering the exceedance probability of limit states in three thresholds: minor (5 cm),

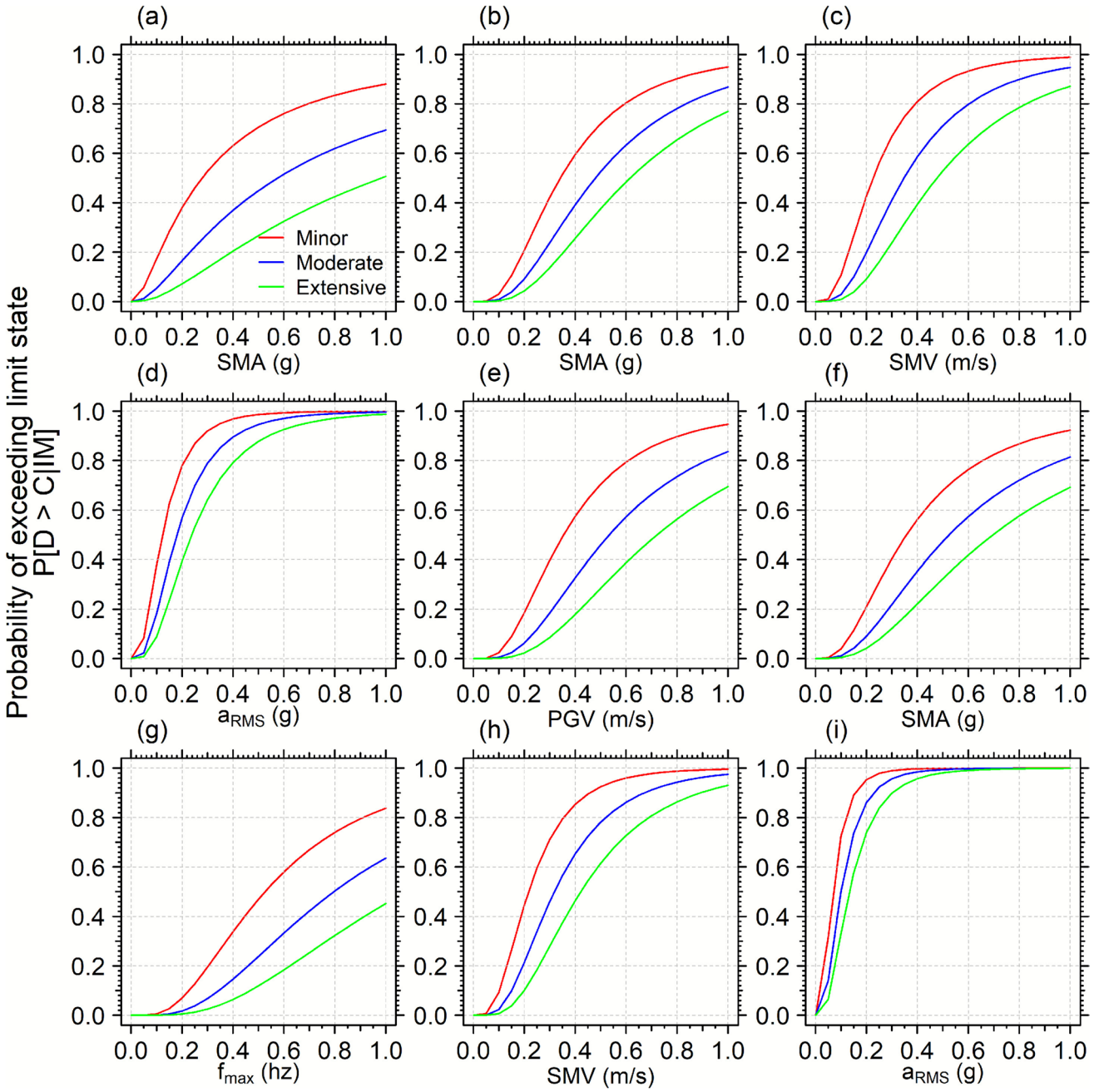

Fig. 15 Fragility curves against the selected intensity measures (IMs) for models at the height of 10 m (**a**), (**d**), and (**g**); 20 m (**b**), (**e**), and (**h**); and 30 m (**c**), (**f**), and (**i**), subjected to set H

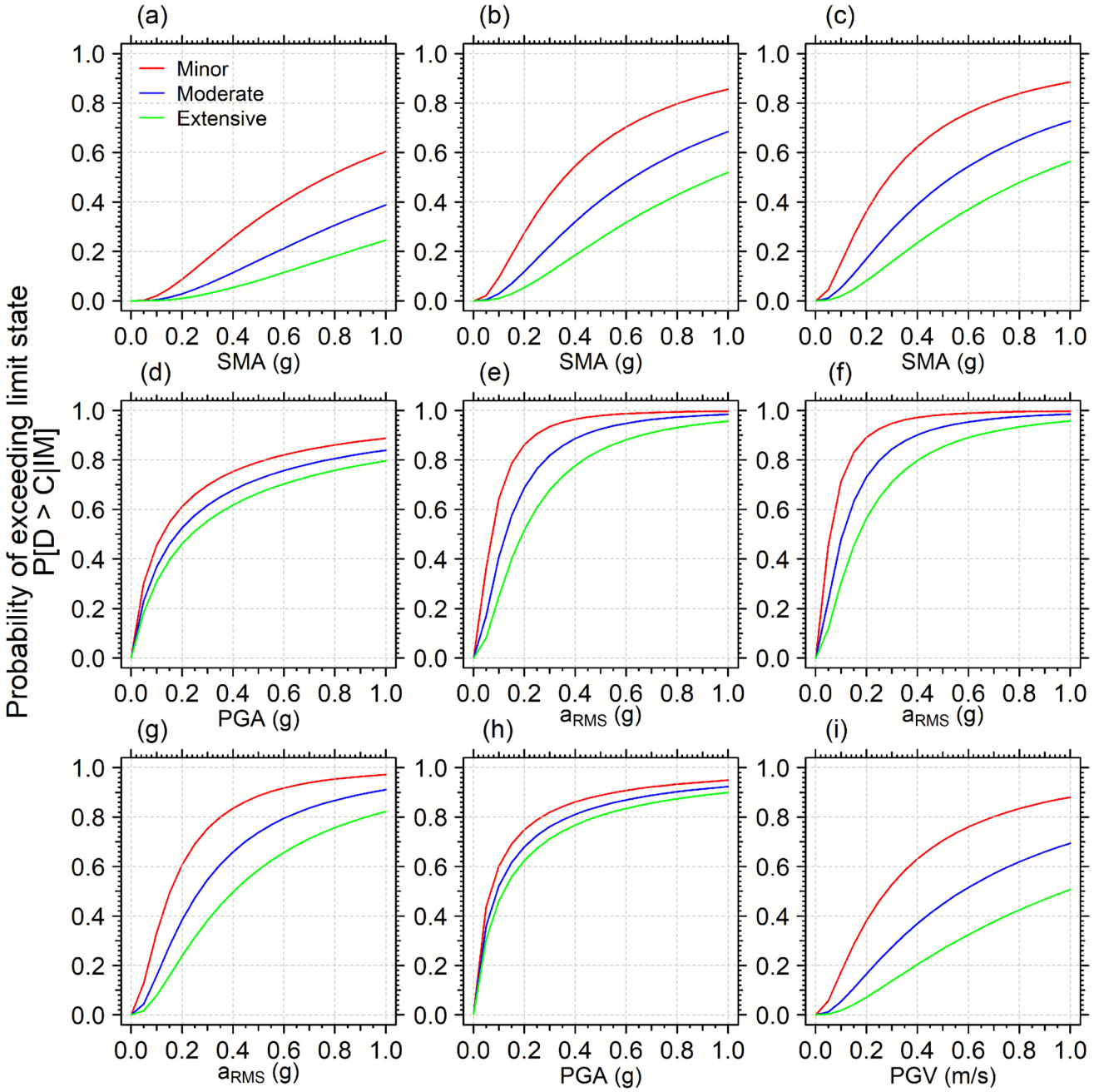

Fig. 16 Fragility curves against the selected intensity measures (IMs) for models at the height of 10 m (**a**), (**d**), and (**g**); 20 m (**b**), (**e**), and (**h**); and 30 m (**c**), (**f**), and (**i**) subjected to set HV

moderate (15 cm), and extensive (30 cm) (Tran et al. 2023). Fragility curves calculate damage probabilities for an IM. Figure 15 shows the values of SMV, SMA, and a_{RMS} of set H with probabilities of 50% (P50) at three limit states of minor, moderate, and extensive for the 30 m model; SMA is 0.36, 0.53, and 0.70 g; SMV is 0.23, 0.35, and 0.48 m/s, while a_{RMS} is 0.07, 0.1, and 0.13 g. The SMA exceeds 34% of the SMV and 81% of the a_{RMS} at 50% failure probability. Set HV and IMs have a similar finding—SMA is the highest, followed by PGV, while a_{RMS} is the lowest at the same P50 for the 30 m model.

6 Conclusion

The optimal IMs for seismic slope stability in PSDMs were examined using the criteria of efficiency, practicality, proficiency, and sufficiency. Three slope models of

H_{slope} =10 m, 20 m, and 30 m were examined with two sets of ground motions including horizontal (H) and H in combination with vertical (V) direction. Selected 19 IMs were computed based on 150 H1, 150 H2, and 150 V components from 61 earthquakes, at a total of 300 H and 300 HV. The optimal IMs predicted D_{max} as an EDP for slopes.

Generally, except for the proficiency criterion, acceleration-related IMs (for example, I_A, I_C, ASI, and EPA) and velocity-related IMs (for example, VSI, SMV, and PGV) are optimal IMs for models subject to sets H and HV. Displacement-related IMs like PGD, RMSD, and CAD are less appropriate. There are no significant variations in optimal IMs between H alone and HV ground motions across the three slope geometries. It is possible to apply the best IM to both H and HV ground motions. We recommend SMA for lower-height slope models (H_{slope} = 10 m and 20 m) and SMV for the highest-height slope model of 30 m under set H; SMA could also be used for the highest model; SMA is the best IM for all three models under set HV, with a_{RMS} being another option. It was surprising that PGA, a common IM for seismic analysis of geotechnical and civil structures, is less effective for both H and HV ground motions in this study.

This study has several limitations. First, the IMs were determined using four criteria without considering hazard evaluation, which should be addressed in future research. Second, the analysis examined slope geometry by altering slope height while maintaining slope angle. The selected heights (10 m, 20 m, and 30 m) may provide important insights, but more examples with different angles of inclination should be included to expand geometry diversity. Given the considerable importance of slope geometry on seismic performance, future study should rigorously investigate slopes with varying inclinations (for example, 30°, 45°, 60°). Moreover, site conditions greatly affect seismic energy transmission and experience by structures, therefore they are critical in choosing PSDM IMs. Variations in soil type, site amplification effects, and local geological characteristics can affect seismic wave behavior, affecting how well different IMs capture seismic threats. Additional research should include site-specific elements to better understand their impact on slope stability. Third, our research is based on a carefully selected 19 IMs, although more can be chosen. Future research should include more IMs to better analyze their possible impact on seismic assessments and strengthen the conclusions in studies. Last, according to Xiao et al. (2024), considering safety and sliding volume EDPs might better explain slope behavior under seismic stress. However, only D_{max} was used as the EDP in this study. Therefore, the incorporation of additional EDPs such as factors of safety or sliding volume in future studies would provide a more holistic understanding of slope behavior under seismic loading.

Acknowledgment This study was funded by the National Natural Science Foundation of China (Grant No. 52422807).

References

Alielahi, H., and M.R. Moghadam. 2016. Fragility curves evaluation for broken-back block quay walls. *Journal of Earthquake Engineering* 21(1): 1–22.

Arias, A. 1970. A measure of earthquake intensity. *Seismic Design for Nuclear Power Plants* 1970: 438–483.

Baker, J.W. 2015. Efficient analytical fragility function fitting using dynamic structural analysis. *Earthquake Spectra* 31(1): 579–599.

Bentley 2022. PLAXIS 2D tutorial manual connect edition V22. Exton, PA: Bentley.

Bentley 2024. PLAXIS 2D-material-models connect edition V24. Exton, PA: Bentley.

Che, W., P. Chang, and W. Wang. 2023. Optimal intensity measures for probabilistic seismic stability assessment of large open-pit mine slopes under different mining depths. *Shock and Vibration*. https://doi.org/10.1155/2023/8851565.

Cornell, C.A., F. Jalayer, R.O. Hamburger, and D.A. Foutch. 2002. Probabilistic basis for 2000 SAC Federal Emergency Management Agency steel moment frame guidelines. *Journal of Structural Engineering* 128(4): 526–533.

Crowley, H., R. Pinho, and J.J. Bommer. 2004. A probabilistic displacement-based vulnerability assessment procedure for earthquake loss estimation. *Bulletin of Earthquake Engineering* 2: 173–219.

Cundall, P., H. Hansteen, S. Lacasse, and P. Selnes. 1980. NESSI: Soil structure interaction program for dynamic and statistic problems. Report 51508-9. Oslo, Norway: Norwegian Geotechnical Institute.

Deierlein, G.G., A.B. Liel, C.B. Haselton, and C.A. Kircher. 2008. ATC 63 methodology for evaluating seismic collapse safety of archetype buildings. In *Structures Congress 2008*, ed. D. Anderson, C. Ventura, D. Harvey, and M. Hoit. Reston, VA: American Society of Civil Engineers.

EU (European Union). 2004. Eurocode8. Design of structures for earthquake resistance. Brussels, Belgium: The EU.

Fotopoulou, S.D., and K.D. Pitilakis. 2015. Predictive relationships for seismically induced slope displacements using numerical analysis results. *Bulletin of Earthquake Engineering* 13(11): 3207–3238.

Hariri-Ardebili, M.A., and V.E. Saouma. 2016. Probabilistic seismic demand model and optimal intensity measure for concrete dams. *Structural Safety* 59: 67–85.

Housner, G. 1975. Measures of severity of earthquake ground shaking. In *Proceedings of the U.S. National Conference on Earthquake Engineering*, 18–20 June 1975, Ann Arbor, Michigan, USA.

Hu, H., and Y. Bao. 2024. Seismic fragility functions for earthquake-induced landslide risk assessment using identified optimal earthquake intensity measures. *CATENA* 234: Article 107589.

Hu, H., Y. Huang, and Z. Chen. 2019. Seismic fragility functions for slope stability analysis with multiple vulnerability states. *Environmental Earth Sciences* 78(24): Article 690.

Irslan Khalid, M., D. Park, J. Fei, V.-Q. Nguyen, D.-D. Nguyen, and X. Chen. 2023. Selection of efficient earthquake intensity measures for evaluating seismic fragility of concrete face rockfill dam. *Computers and Geotechnics* 163: Article 105721.

Khalid, M.I., J. Fei, D.-h. Lee, D. Park, and X. Chen. 2024. Probabilistic assessment of seismic performance of slopes considering the sensitivity of sliding surface to input motion. *Soil Dynamics and Earthquake Engineering* 182: Article 108737.

Kim, J.M., and N. Sitar. 2013. Probabilistic evaluation of seismically induced permanent deformation of slopes. *Soil Dynamics and Earthquake Engineering* 44: 67–77.

Kim, C., H.D. Nguyen, M. Shin, and J.M. LaFave. 2025. Fragility analysis of APR-1400 nuclear containment structures under internal pressure. *Nuclear Engineering and Design* 433: Article 113864.

Kramer, S.L. 1996. *Geotechnical earthquake engineering*. Upper Saddle River, NJ: Prentice-Hall Inc.

Kumar, S., S.S. Choudhary, and A. Burman. 2023. The effect of slope height and angle on the safety factor and modes of failure of 3D slopes analysis using limit equilibrium method. *Beni-Suef University Journal of Basic and Applied Sciences* 12(1): Article 84.

Kurama, Y.C., and K.T. Farrow. 2003. Ground motion scaling methods for different site conditions and structure characteristics. *Earthquake Engineering & Structural Dynamics* 32(15): 2425–2450.

Kwok, J.P.S., Y.M.A. Hashash, N. Matasovic, R. Pyke, Z. Wang, and Z. Yang. 2007. Use of exact solutions of wave propagation problems to guide implementation of nonlinear seismic ground response analysis procedures. *Journal of Geotechnical and Geoenvironmental Engineering* 133(11): Article 1385.

Latha, G.M., and A. Garaga. 2010. Seismic stability analysis of a Himalayan rock slope. *Rock Mechanics and Rock Engineering* 43(6): 831–843.

Lysmer, J., and R.L. Kuhlemeyer. 1969. Finite dynamic model for infinite media. Department of Civil Engineering, University of California, Berkeley, CA, USA.

Mackie, K., and B. Stojadinović. 2001. Probabilistic seismic demand model for California highway bridges. *Journal of Bridge Engineering* 6(6): Article 468.

Malhotra, P.K. 1999. Response of buildings to near-field pulse-like ground motions. *Earthquake Engineering & Structural Dynamics* 28(11): 1309–1326.

Maruyama, Y., F. Yamazaki, K. Mizuno, Y. Tsuchiya, and H. Yogai. 2010. Fragility curves for expressway embankments based on damage datasets after recent earthquakes in Japan. *Soil Dynamics and Earthquake Engineering* 30(11): 1158–1167.

McCartney, J.S., H. Yu, E. Ntambakwa, B. Mendes, and I. Tomac. 2020. Comparison of 1-D seismic site response analysis tools for layered liquefiable deposits at an offshore windfarm site. *E3S Web of Conferences* 205: Article 12005.

Meko, L., Y.C. Chemeda, and B. Meko. 2023. Road cut slope stability analysis for static and dynamic (pseudo-static analysis) loading conditions. *Open Geosciences* 15: Article 20220561.

Murthy, T.N., and G.R. Patil. 2015. Effect of vertical ground motion on reinforced concrete structures. *Mechanical and Civil Engineering* 12: 33–39.

Nguyen, H.D., N.D. Dao, and M. Shin. 2021. Prediction of seismic drift responses of planar steel moment frames using artificial neural network and extreme gradient boosting. *Engineering Structures* 242: Article 112518.

Nguyen, H.D., C. Kim, Y.-J. Lee, and M. Shin. 2024. Incorporation of machine learning into multiple stripe seismic fragility analysis of reinforced concrete wall structures. *Journal of Building Engineering* 97: Article 110772.

Nguyen, H.D., Y.-J. Lee, J.M. LaFave, and M. Shin. 2023. Seismic fragility analysis of steel moment frames using machine learning models. *Engineering Applications of Artificial Intelligence* 126: Article 106976.

Nguyen, H.D., M. Shin, and J.M. LaFave. 2023. Optimal intensity measures for probabilistic seismic demand models of steel moment frames. *Journal of Building Engineering* 65: Article 105629.

Nguyen, H.D., M. Shin, and M. Torbol. 2020. Reliability assessment of a planar steel frame subjected to earthquakes in case of an implicit limit-state function. *Journal of Building Engineering* 32: Article 101782.

NIBS (National Institute of Building Sciences) and FEMA (Federal Emergency Management Agency). 2003. HAZUS-MH MR4 technical manual. Washington, DC: NIBS and FEMA.

Nuttli, O.W. 1979. *The relation of sustained maximum ground acceleration and velocity to earthquake intensity and magnitude*. Vicksburg, MI: U.S. Army Engineer Waterways Experiment Station.

Özmen, B.O. 2019. Modelling the variability in seismically induced slope displacements due to ground motion selection. https://etd.lib.metu.edu.tr/upload/12623183/index.pdf. Accessed 22 Jul 2020.

Padgett, J.E., and R. DesRoches. 2008. Methodology for the development of analytical fragility curves for retrofitted bridges. *Earthquake Engineering & Structural Dynamics* 37(8): 1157–1174.

Padgett, J.E., B.G. Nielson, and R. DesRoches. 2007. Selection of optimal intensity measures in probabilistic seismic demand models of highway bridge portfolios. *Earthquake Engineering & Structural Dynamics* 37(5): 711–725.

Park, Y.-J., A.H.-S. Ang, and Y.K. Wen. 1985. Seismic damage analysis of reinforced concrete buildings. *Journal of Structural Engineering* Ill(4): Article 705.

Pushpa, K., S.K. Prasad, and P. Nanjundaswamy. 2016. Critical analysis of slope stability analysis methods. *International Journal of Engineering Research & Technology (IJERT)* 5(7): 128–136.

Rathje, E.M., and G. Saygili. 2009. Probabilistic assessment of earthquake-induced sliding displacements of natural slopes. *Bulletin of the New Zealand Society for Earthquake Engineering* 42(1): 18–27.

Reed, J.W., and R.P. Kassawara. 1990. A criterion for determining exceedance of the operating basis earthquake. *Nuclear Engineering and Design* 123(2): 387–396.

Riddell, R., and J.E. Garcia. 2001. Hysteretic energy spectrum and damage control. *Earthquake Engineering & Structural Dynamics* 30(12): 1791–1816.

Saygili, G., and E.M. Rathje. 2008. Empirical predictive models for earthquake-induced sliding displacements of slopes. *Geotechnical and Geoenvironmental Egineering* 134: 790–803.

Saygili, G., and E.M. Rathje. 2009. Probabilistically based seismic landslide hazard maps: An application in Southern California. *Engineering Geology* 109(3–4): 183–194.

Shome, N., C.A. Cornell, P. Bazzurro, and J.E. Carballo. 1998. Earthquakes, records, and nonlinear responses. *Earthquake Spectra* 14(3): 469–500.

Stokoe, II, K.H., M.B. Darendeli, R.B. Gilbert, F.-Y. Menq, and W.K. Choi. 2001. Development of a new family of normalized modulus reduction and material damping curves. https://apps.peer.berkeley.edu/lifelines/Workshop304/pdf/Stokoe_PlenaryPaper.pdf. Accessed 20 Nov 2020.

Thun, J., L.H. Roehm, G.A. Scott, and J.A. Wilson. 1988. Earthquake ground motions for design and analysis of dams. *Geotechnical Special Publication* 20: 463–481.

Tidke, A.R., and S. Adhikary. 2022. Optimal intensity measure selection and probabilistic seismic demand models for dam-reservoir-layered foundation system. *Structures* 37: 318–337.

Tothong, P., and N. Luco. 2007. Probabilistic seismic demand analysis using advanced ground motion intensity measures. *Earthquake Engineering & Structural Dynamics* 36(13): 1837–1860.

Tran, D.T.P., Y. Cho, H. Seo, and B. Kim. 2023. Seismic fragility assessments of fill slopes in South Korea using finite element simulations. *Geomechanic and Engineering* 34: 341–380.

Travasarou, Th., and J.D. Bray. 2003. Optimal ground motion intensity measures for assessment of seismic slope displacements. In *Proceedings of the 2003 Pacific Conference on Earthquake Engineering*, 13–15 February 2003, University of Canterbury, Christchurch, New Zealand.

Trifunac, M.D., and A.G. Brady. 1975. On the correlation of seismic intensity scales with the peaks of recorded strong ground motion. *Bulletin of Seimological Society of America* 65: 139–162.

Tsompanakis, Y., N.D. Lagaros, P.N. Psarropoulos, and E.C. Georgopoulos. 2010. Probabilistic seismic slope stability assessment of geostructures. *Structure and Infrastructure Engineering* 6(1–2): 179–191.

Wang, H., M. Jia, Y. Yao, X. Chen, and Z. Zhang. 2023. Influence of the vertical component of Yangbi ground motion on the dynamic response of RC frame and brick-concrete structure. *Buildings* 13(1): Article 147.

Wen, Y.K., B.R. Ellingwood, and J. Bracci. 2004. Vulnerability function framework for consequence-based engineering. https://www.researchgate.net/publication/32962749_Vulnerability_Function_Framework_for_Consequence-Based_Engineering. Accessed 1 Jan 2022.

Wibowo, H., and S. Sritharan. 2022. Effects of vertical ground acceleration on the seismic moment demand of bridge superstructure connections. *Engineering Structures* 253: Article 113820.

Wu, X.Z. 2014. Development of fragility functions for slope instability analysis. *Landslides* 12(1): 165–175.

Xiao, Y., Y. Zhang, X. Cheng, and C. Xiang. 2024. Dynamic response and seismic vulnerability assessment of the near-fault steep slope. *Soil Dynamics and Earthquake Engineering* 183: Article 108794.

Zhang, Y.B., G. Chen, J. Wu, L. Zheng, and X. Zhuang. 2012. Numerical simulation of seismic slope stability analysis based on tension-shear failure mechanism. *Geotechnical Engineering* 43(2): 18–28.

Zhang, C., M. Zhao, Z. Zhong, and X. Du. 2022. Optimum intensity measures for probabilistic seismic demand model of subway stations with different burial depths. *Soil Dynamics and Earthquake Engineering* 154: Article 107138.